

We are IntechOpen, the world's leading publisher of Open Access books Built by scientists, for scientists

6,900

Open access books available

185,000

International authors and editors

200M

Downloads

Our authors are among the

154

Countries delivered to

TOP 1%

most cited scientists

12.2%

Contributors from top 500 universities



WEB OF SCIENCE™

Selection of our books indexed in the Book Citation Index
in Web of Science™ Core Collection (BKCI)

Interested in publishing with us?
Contact book.department@intechopen.com

Numbers displayed above are based on latest data collected.
For more information visit www.intechopen.com



Doped Zinc Oxide Nanostructures for Photovoltaic Solar Cells Application

Tyona MD

Abstract

Zinc oxide and doping effects of Cu on its structural, morphological, optical, and surface wettability properties and the consequent influence on photoelectrochemical solar cell performance has been reviewed. Cu dopant in the doping solution is varied in the range of 1 to 5 at.% which significantly affected the properties of ZnO. Slight changes in the lattice parameters of the Cu-doped zinc oxide (CZO) electrodes were reported, due to the successful substitution of Zn^{2+} by Cu^{2+} and also enhancement in crystallinity of the films at 3 at.% Cu due to reduction in crystallographic defects in the film. Surface morphologies were reported with densely grown nanorods over the varied range of Cu, with 3 at.% having the densest microstructures with average diameter approximately 125 nm. A review of optical properties indicated significant enhancement in absorption edge of approximately 60 nm into the visible band for the nanorods with 3 at.% Cu content due to light scattering. Optical energy band-gaps decrease from 3.03 to 2.70 eV with Cu doping. Surface wettability was adjudged hydrophilic for all the films, implying high porosity and water contact angles depended on Cu content. Photoelectrochemical cell performance indicated an n-type photoactivity in sodium sulfate (Na_2SO_4) electrolyte, which motivates to check its feasibility in solar cell applications.

Keywords: zinc oxide, nanostructures, CZO, photoelectrochemical solar cells, Cu concentration, nanorods

1. Introduction

Zinc oxide is an inorganic compound having a chemical formula ZnO . It is a white powder which is nearly insoluble in water. It crystallizes in two main forms, the hexagonal wurtzite and cubic zinc blende. The wurtzite structure with lattice parameters $a = 0.3296$ and $c = 0.52065$ nm is found to be more stable than the zinc blende structure, and hence it is more widely used [1]. The ZnO structure is commonly described as consisting of a number of alternating planes composed of tetrahedrally coordinated O^{2-} and Zn^{2+} ions, stacked alternately along the c -axis without a central symmetry as illustrated in **Figure 1** [1, 2]. It is a group II–VI semiconductor with a wide band gap of about 3.33 eV. Due to its direct and wide band gap in the near-UV spectral region [3–5] and a large free exciton binding energy, it has become a promising functional semiconductor material, which possesses a wide range of novel applications. ZnO has been identified with many unique properties

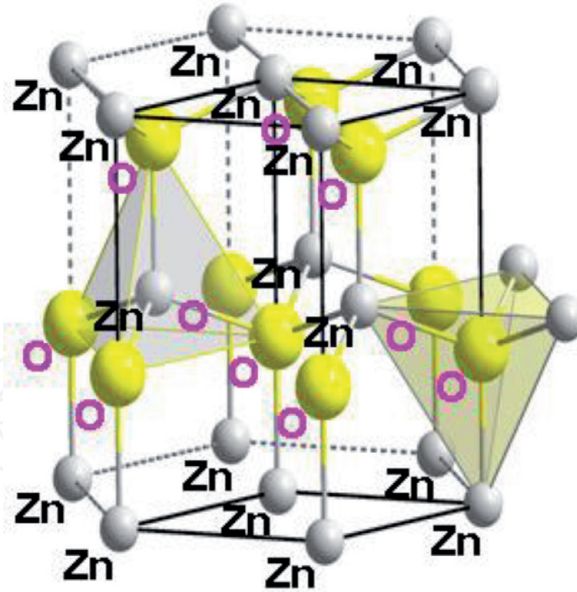


Figure 1.
Hexagonal Wurtzite crystal structure of ZnO [1].

such as excitonic emission at or even above room temperature, optical transparency in the visible range, high surface-to-volume ratio and quantum confinement effect [6], amongst others, which have motivated intensive study of the semiconductor during the last two decades. ZnO is mostly known to crystalize as an n-type semiconductor, whereas synthesis of the p-type is not generally easy [1, 7].

ZnO is simple to synthesize; both chemical and physical techniques are used to produce excellent epitaxial films. The most commonly used techniques to grow epitaxial films of ZnO include electrodeposition, spray pyrolysis, sol-gel process, successive ionic layer adsorption and reaction (SILAR), RF sputtering, chemical bath deposition (CBD), spin coating, electron beam epitaxy, laser evaporation and ion beam sputtering, amongst others [7, 8]. **Figure 2** illustrates the various synthetic techniques (chemical as well as physical) that are generally used to grow compound and alloys of ZnO. The choice of a particular technique would be guided by some factors such as the application intended for the synthesis, effectiveness of the technique and cost implication [10, 11]. ZnO has been identified as one of the semiconductors with the largest number of novel nanostructures such as nanocombs, nanorings, nanohelices/nanosprings, nanobelts, nanowires, nanorods, nanotubes, nanocages, etc., with a wide range of technological applications [12–15]. Novel applications of ZnO nanostructures include optical modulator waveguide, photonic crystals, surface acoustic wave filters, varistors, photodetectors, gas sensors, light-emitting diode, photodiodes and solar cells, amongst others [12].

Photovoltaic (PV) application of ZnO nanostructures requires large internal surface area with porous and high surface roughness to support good penetration of electrolyte [13, 14]. Chemical techniques are very simple, much reliable and cost-effective for the synthesis of high-quality electrodes for PV application. Most especially, chemical bath deposition technique is very suitable for growing large area films of ZnO with fascinating properties for photoelectrochemical solar cells [15, 16]. This technique is suitable for growing ZnO nanostructures on many substrates including microscope glass and stainless steel [6].

In several applications such as optoelectronics, ZnO can be used as a complement or alternative to some semiconductors such as GaN, and many researches are ongoing globally to further improve the properties of the semiconductor [10]. Trying to control the unintentional n-type conductivity and to achieve p-type

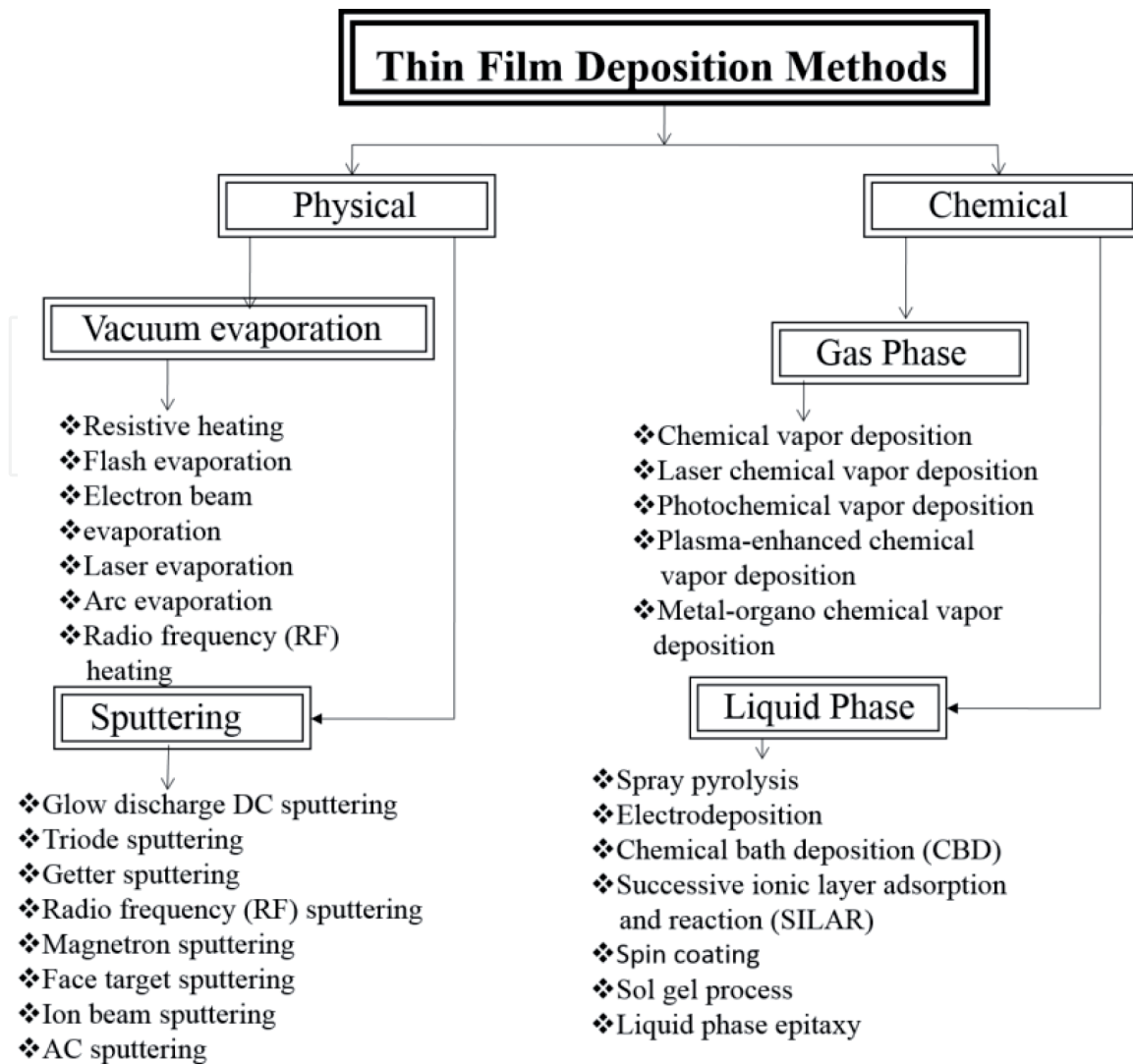


Figure 2.
 Broad classification of thin film deposition techniques [9].

conductivity are such famous research themes. Other approaches such as first-principles calculations based on density functional theory (DFT) are theoretical and, however, are useful to provide in-depth understanding of the role of native point defects and impurities on the unintentional n-type conductivity in ZnO [14, 17]. Acceptor doping in ZnO which will lead to stable p-type is not yet well known [18].

It has been noted that wide application of ZnO in electronic devices has been limited by the lack of inadequate control over its electrical conductivity [10, 19]. Controlling the conductivity in ZnO can be achieved by means of band-gap engineering [10]. Introducing small concentrations of native point defects and impurities (dopants) (down to $10\text{--}14\text{ cm}^{-3}$ or 0.01 ppm) can significantly affect the electrical, structural, optical and morphological properties of the semiconductors [14, 18]. Therefore, understanding the role of native point defects (i.e. vacancies, interstitials and antisites) and the incorporation of impurities (doping) is the key towards controlling the conductivity in ZnO, which in effect alters the band gap, thus enhancing its performance [1].

Band-gap engineering of ZnO can also be achieved by alloying with MgO or CdO. The band gap of ZnO is increased with the addition of Mg, whereas the addition of Cd decreases the band gap, which is similar to the effects of Al and In in GaN [1, 18]. It is well known that MgO and CdO crystallize in the rock salt structure;

however, alloys of $\text{Mg}_{1-x}\text{Zn}_x\text{O}$ and $\text{Cd}_{1-x}\text{Zn}_x\text{O}$ with moderate concentrations will assume the wurtzite structure of the parent compound with significant band-gap variation [1]. This chapter will carry out a detailed review of the doping effects of Cu, Al and In on ZnO and the influence of the doped electrodes on the PEC solar cell performance.

2. Doping as a technique for engineering structural, optical and morphological properties of ZnO

Doping implies the deliberate inclusion of impurities into the crystal structure of a semiconductor in order to improve its conductivity and modify some of its characteristics [19]. For elemental semiconductors such as silicon and germanium, the commonly used dopants include boron, aluminum and indium (trivalent elements) and phosphorus, arsenic and antimony (pentavalent element) [20]. In the process of doping, the dopant is integrated into the lattice structure of the semiconductor crystal. The number of valence electrons of the dopant defines the type of doping that would be achieved [20]. Doping a semiconductor with a trivalent element results into p-type doping, whereas using a pentavalent element produces an n-type doping as illustrated in **Figure 3**. For an n-doping, electrons are the majority charge carriers, while holes are the majority carriers in p-doping. The conductivity of a silicon crystal which is properly doped can be increased by a factor of 10^6 [1].

Compound semiconductors such as ZnO can also be doped with the same or similar dopants like copper and indium. There are reports in the literature on the modification of structural, morphological and optical properties of ZnO by doping with Al, Cu or In. Cu and In dopants have been confirmed to lower the band gap of ZnO appreciably [10, 18].

Doped semiconductors are electrically neutral. The terms n- and p-type doped do only refer to the majority charge carriers. Each positive or negative charge carrier belongs to a fixed negative or positive charged dopant as illustrated in **Figure 4**.

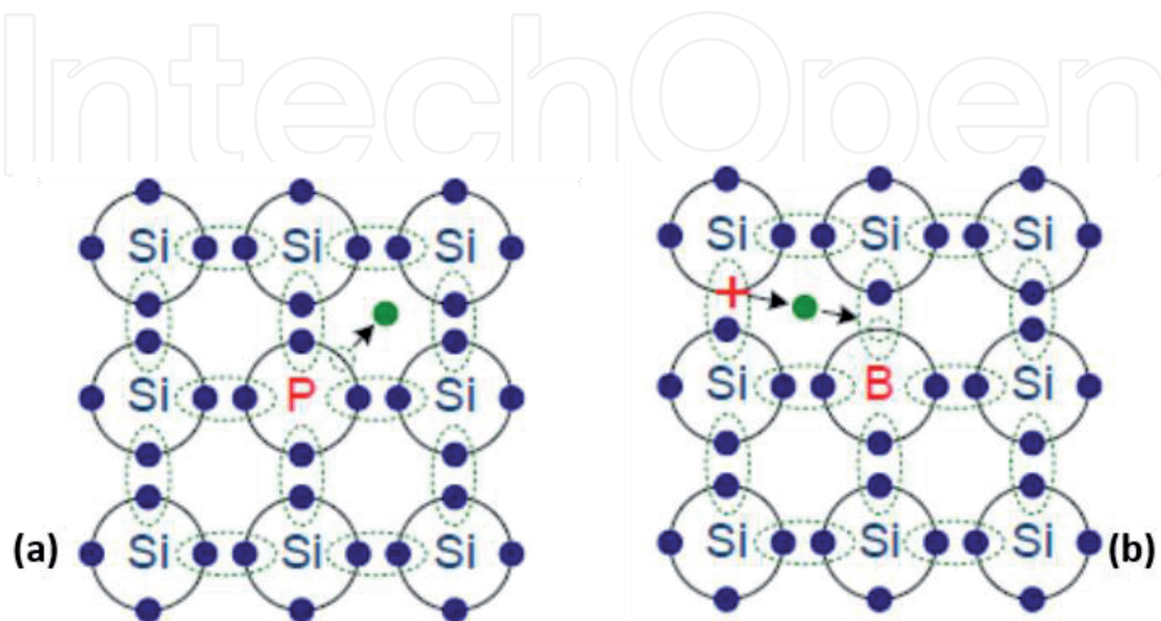


Figure 3.
(a) N-doping with phosphorus and (b) p-doping with boron [2].

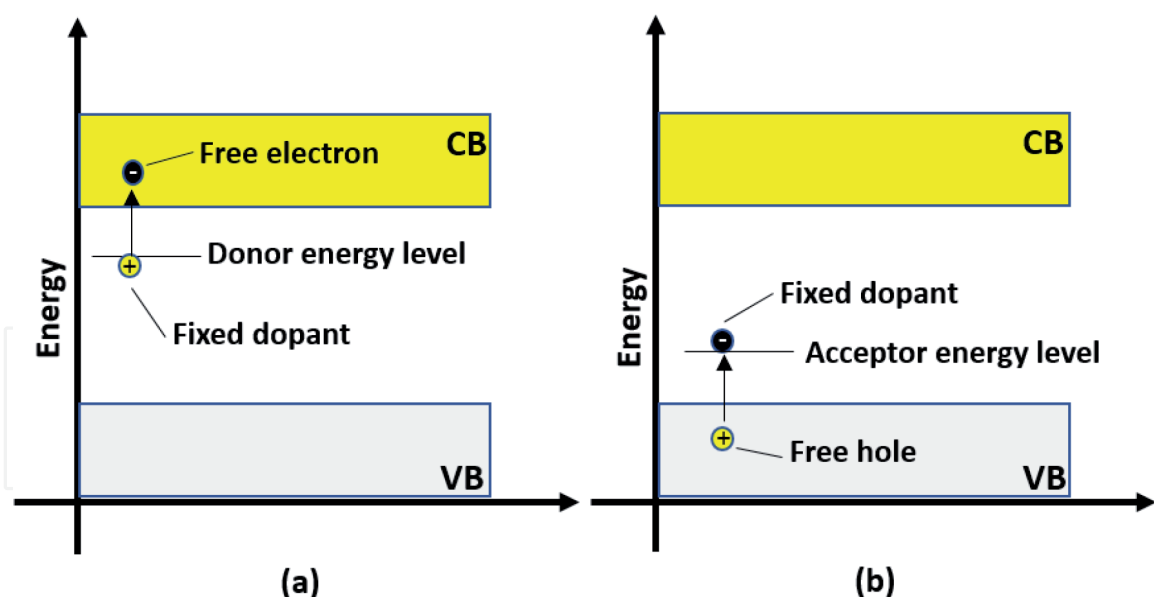


Figure 4.
 Doped semiconductor showing energy levels of (a) n-type doping (b) p-type doping [20].

3. Effects of Cu dopant on ZnO and the PEC solar cell performance of Cu-doped ZnO (CZO) electrodes

Wide band-gap semiconductors such as ZnO and TiO_2 (3.3 eV) are suitable for many semiconductor applications such as PEC solar cells due to their thermal, photo- and electrochemical stability and resistance against atmospheric corrosion [21]. However, the wide band gap in such semiconductors is a drawback on their light absorption capability because only photons below a threshold wavelength λ_g can be absorbed, since the solar spectrum has its maximum intensity at about 2.7 eV [19]. Previous investigations have confirmed that band gap in ZnO semiconductor can be controlled by doping with appropriate dopants [10]. This can also modify optical and structural properties of the semiconductor to meet pre-desired applications [19].

Transitional metals are good dopants; however, Cu and Al are prevalently studied as dopants for ZnO [18]. Cu is a highly conducting metal with conductivity higher than that of Al and can enhance green luminescence band through creation of localized states in the band gap of ZnO. It is also known that due to the high ionization energy and low formation energy of Cu, it can rapidly substitute Zn in ZnO lattice [22].

Tyona et al. [10] investigated the effect of Cu doping on optoelectronic properties of chemically synthesized ZnO electrodes. These properties of Cu-doped ZnO nanostructures were influenced by various parameters such as growth conditions, Cu concentration and post-growth annealing. Cu concentration in ZnO was varied in the range of 1–5%. This quantity may be small; however, it produces significant physical changes in ZnO, and it is considered to be within a strict doping range of up to 10%. Beyond this range, such a reaction may be turning towards composite growth or alloys [10].

Their experimental procedures showed that $\text{Zn}(\text{NO}_3)_2 \cdot 6\text{H}_2\text{O}$ (SD Fine Chemicals) was used as the source of Zn^{2+} and $\text{CuCl}_2 \cdot 2\text{H}_2\text{O}$ (Chemco Fine, India) as the source of Cu^{2+} , and NH_3 solution (28%) (Thomas Baker) was the complexing agent. An aqueous solution of 0.1 M $\text{Zn}(\text{NO}_3)_2 \cdot 6\text{H}_2\text{O}$ was prepared, and cupric chloride dihydrate ($\text{CuCl}_2 \cdot 2\text{H}_2\text{O}$) was added. Aqueous NH_3 solution (28%) was used as the complexing agent. The solution was maintained at a pH \approx 11.5. Microscopic

glass slides and stainless steel slides were used as substrates and immersed vertically in the solution using Bakelite holder at a bath temperature of 353 K. The substrates were coated with CZO thin films, well adherent to the substrates after 5 h, washed, dried in air and preserved in a vacuum desiccator. Further, as-deposited films were air annealed at 673 K for 2 h and characterized using the following techniques: X-ray diffraction (XRD) patterns were obtained with Cu K α ($\lambda = 1.5406 \text{ \AA}$) radiation from a Philips X-ray diffractometer, Philips PW1830, in the range 20–80°. The morphology of the CZO thin films was measured with the scanning electron microscope (SEM) using JEOL JSM-6360. Optical properties were studied using Shimadzu UV-1800 spectrophotometer in the range 300–800 nm. Contact angle meter (ramé-hart USA equipment) with CCD camera was used to measure the surface wettability of the films. PEC activities of CZO films were studied by forming cells with n-CZO (stainless steel substrate)/0.1 M Na₂SO₄/platinum/SCE, which were illuminated with an 80 mW/cm² xenon arc lamp [10]. They analyzed their results under the following headings:

3.1 Film formation mechanism

In their results, they examined CZO film formation process by chemical bath deposition method under four steps of particle growth [10] as in **Figure 5**: (a) nucleation, (b) aggregation, (c) coalescence and, subsequently, (d) growth by stacking of the particles (**Figure 5e**). It is noted that during growth process, the diameter and density of ZnO nanorod are highly affected by the density of the nucleation sites and the pH value of the aqueous solution. Therefore, introducing Cu impurities into the reaction path would increase the nucleation density and hence enhance the growth rate, which, in turn, results in a coarsening and lateral aggregation of the nanorods [10]. This is apparently due to the fact that Cu²⁺

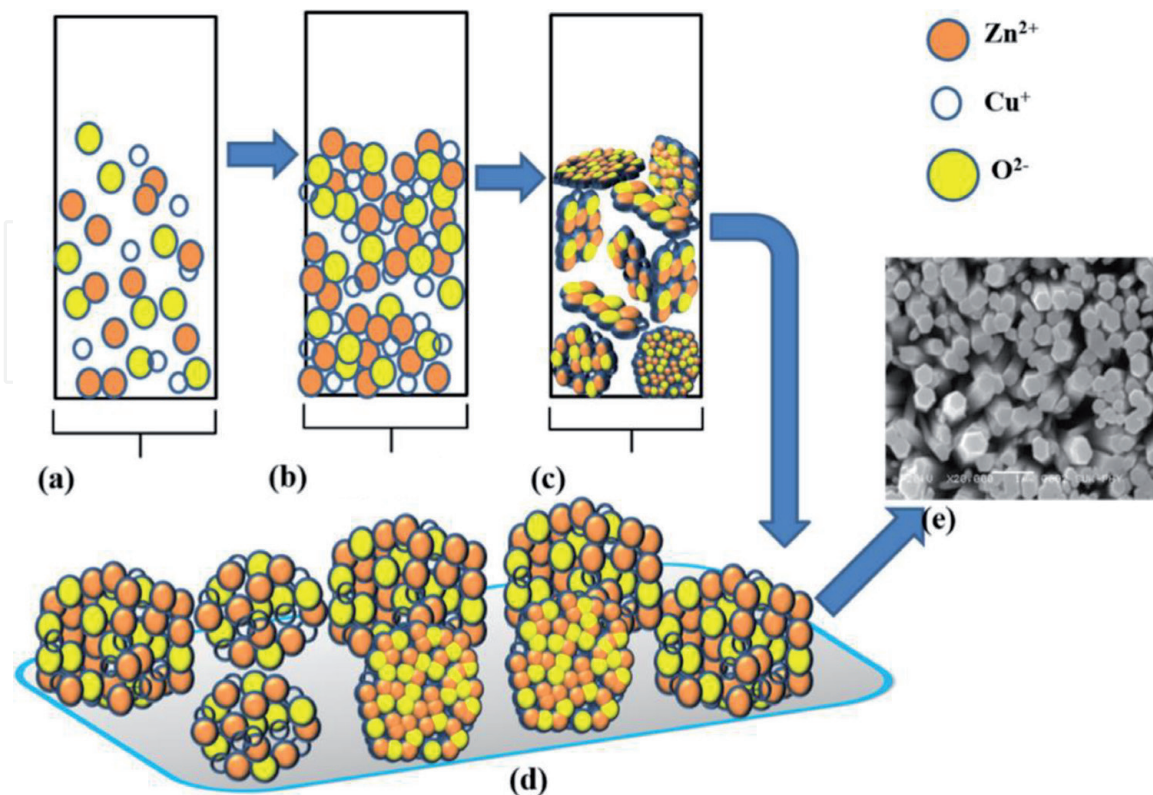
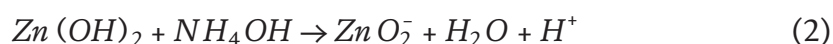


Figure 5. The schematic growth model for the formation of CZO thin films: (a) nucleation, (b) aggregation, (c) coalescence, (d) subsequent growth by stacking of the particles and (e) surface view of grown stacked nanostructures [10].

increases the number of free metal ions in the solution which forms nucleation sites and the highly alkaline medium helps to speed up the release of chalcogenide ions in the solution which cause the increase in film growth rate. During nucleation, the heterogeneous reaction at the substrate surface takes place when molecule clusters begin to undergo rapid decomposition and particles combine to grow up to a certain thickness of the film [10]. For deposition of ZnO, $\text{Zn}(\text{NO}_3)_2 \cdot 6\text{H}_2\text{O}$ was used as a source of Zn^{2+} ions. When ammonia was added to it, white precipitate of $\text{Zn}(\text{OH})_2$ occurred, and further $\text{Zn}(\text{OH})_2$ redissolved into the solution by addition of excess ammonia which results into formation of zinc tetra amino complex ($[\text{Zn}(\text{NH}_3)_4]^{2+}$). The decomposition of $[\text{Zn}(\text{NH}_3)_4]^{2+}$ releases Zn^{2+} ions, which reacts with OH^- ions in the solution and results in the formation of $\text{Zn}(\text{OH})_2$ or ZnO particles. The possible reaction mechanism for the formation of ZnO thin films is as follows [10]:



When the solution is heated to 353 K, the ionic product exceeds the solubility product, and precipitation occurred on the glass substrate and in the solution to form ZnO nuclei; thus, ZnO film is formed on the substrate by the following reaction [10]:



The growth process of Cu-doped ZnO proceeded in a similar manner as that of undoped ZnO since doping is a physical process and does not significantly affect the chemical structure of the parent precursor, ZnO.

3.2 Structural characterization

Their CZO electrodes were characterized by X-ray diffraction which revealed that all the film samples were polycrystalline with hexagonal wurtzite structure with lattice constants $a = 3.24982 \text{ \AA}$ and $c = 5.20661 \text{ \AA}$ corresponding to those of the ZnO patterns from the JCPDS data card no: 00-036-1451. A strong preferential growth was seen along the Z-direction for the undoped ZnO and CZO films with 3% Cu concentration, which diminishes significantly for 1 and 5% Cu concentrations as illustrated in **Figure 6**. The decrease in intensity of the ZnO peaks upon incorporation of Cu impurities (i.e. Cu/Zn of 1%) was assigned to induce crystallographic defects on ZnO lattices by Cu dopant which reduced the crystalline quality of the film. They observed on the other hand that raising Cu content to 3% enhances the carrier concentration and mobility in the conduction band of the semiconductor [10], thereby lowering the amount of crystallographic defects in the film and increasing the crystalline quality of the film along the ZnO (002) plane [13]. Further increase in Cu content to 5% lowered the crystalline quality of the film sample significantly as indicated in **Figure 6**, which is an indication of more compressive strain in the films at higher doping level [1, 2].

Barna and Adamik structure zone model for polycrystalline metallic films [23, 24] explained the above-described phenomenon; thus as the Cu content in ZnO is raised, segregation occurred at the grain boundaries in the film, which give rise to shrinkage of crystallite sizes [23]. Therefore, 3% Cu concentration could be the optimum concentration of Cu in ZnO to provide the best crystalline quality film in CZO thin films. This observation slightly defers from an earlier report of Babikier et al. and Mkawi et al. [22, 25] even though they used different concentrations of Cu.

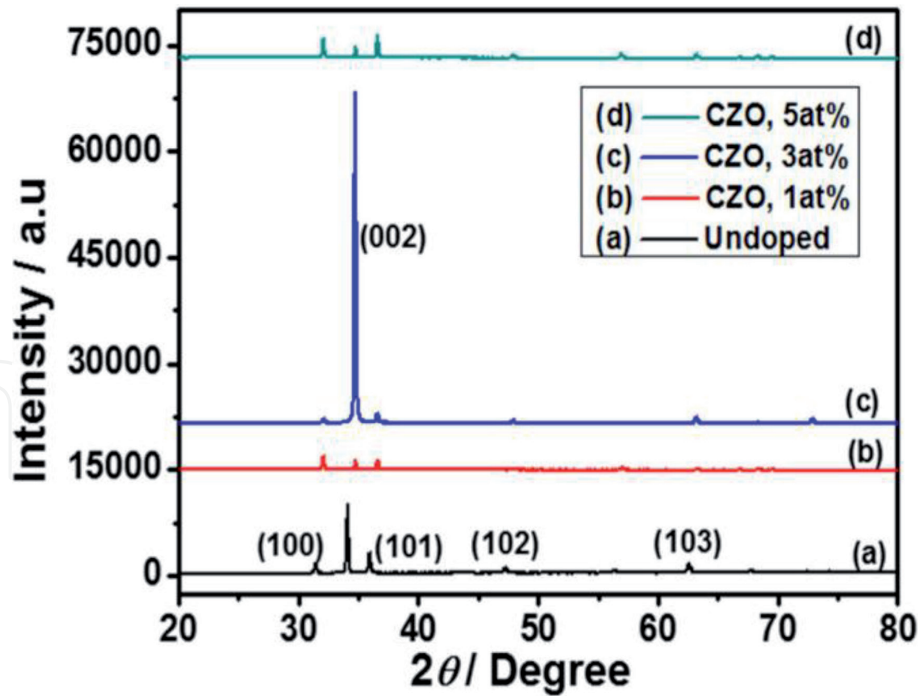


Figure 6. XRD patterns of CZO with varying Cu concentrations: (a) 0%, (b) 1%, (c) 3% and (d) 5% [10].

Another interesting observation here is a shift in angular peak positions of 0.54° in (2θ) along the (002) plane in ZnO when Cu impurities were introduced. This may be assigned to difference in the ionic radii of Zn^{2+} and Cu^{2+} (which is higher for Zn^{2+} as compared to Cu^{2+}) as Cu^{2+} substitutes Zn^{2+} on Zn sites in ZnO, the crystal lattice, thus causing shortening of the c-axis [23]. According to Shannon [24], the fourfold coordinated Zn^{2+} and Cu^{2+} cations have ionic radii of 0.074 and 0.057 nm, respectively, and stable electronic configurations of Zn^{2+} (3d10) and Cu^{2+} (3d9). The fourfold coordinated Cu^{1+} has ionic radius of 0.06 nm Cu^{1+} (3d10) [24].

The mean crystallite sizes, D of the CZO thin films along the c-axis (002), were estimated on the basis of full width at half maxima (FWHM) using Scherrer’s formula [25]:

$$D = \frac{0.9\lambda}{\beta \cos \theta} \tag{4}$$

where λ , β and θ are the X-ray wavelength ($\lambda = 1.54 \text{ \AA}$), full width at half maximum and diffraction peak angle, respectively. Their estimated crystallite sizes indicated a slight increase from 28 to 30 nm as depicted in **Table 1**.

In chemically synthesized ZnO thin film, as-deposited films may likely contain hydroxide and other impurities [25], so thermal annealing is necessary. Thermal annealing causes remarkable changes in the surface morphology of chemically synthesized thin films. Tyona et al. [10] reported the surface morphology of their

| % Doping of Cu | Mean crystallite size (nm) |
|----------------|----------------------------|
| 0 | 28 |
| 1 | 7 |
| 3 | 30 |
| 5 | 8 |

Table 1. Estimated crystallite sizes of CZO thin films using (002) crystal plane [10].

CZO thin films which was studied using scanning electron microscope, JEOL JSM-6360. **Figure 7a–d** depicts the SEM micrographs, with undoped ZnO (as reference) and CZO thin films (as-deposited and annealed) with different Cu concentrations

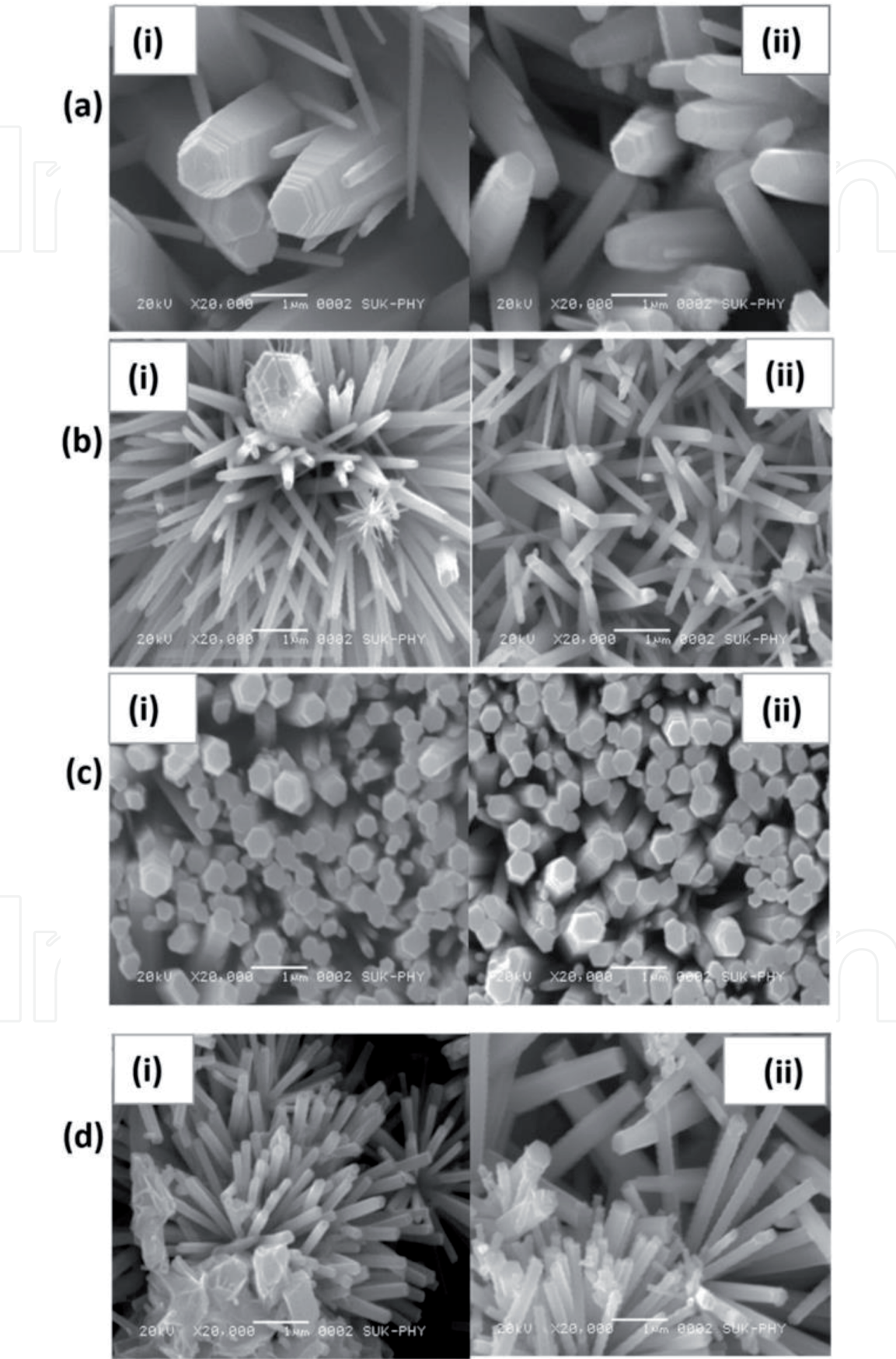


Figure 7.
SEM micrographs of CZO thin films showing as-deposited and annealed samples for various Cu contents.
(a) 0%, as-deposited and annealed. (b) 1%, as-deposited and annealed. (c) 3%, as-deposited and annealed.
(d) 5%, as-deposited and annealed [10].

(0, 1, 3 and 5%). The SEM micrographs showed that the surface morphology of the films was affected by the concentration of the dopant. The crystallite size of the films decreases upon introduction of the Cu impurity as suggested by XRD study except for 3%. This behaviour could also be assigned to the difference in the ionic radii of Zn and the doping element, Cu. Further, with increasing Cu concentration (up to an optimum concentration of 3%), the microstructures of the film became denser as in **Figure 7c**. **Figure 7a(i)** and **(ii)** illustrates SEM micrographs of the undoped ZnO thin films (as-deposited and annealed) identified with randomly oriented nanorods of average diameter approximately 125 nm.

3.3 Surface morphological studies

The micrograph of the as-deposited CZO (i.e. 1%) film as depicted in **Figure 7b(i)** showed surface morphology with well-defined nanorods grown randomly on the substrate as thin solid films of Cu-Zn(OH)₂ with sparsely distributed needle-like images attached to some rods. Each rod is crystalline and indexed to hexagonal crystal structure, as seen in **Figure 7b(i)**. The average diameter of the rods was of the order of ≈ 40 nm. After annealing at 673 K, the nanorods.

Were refined to CZO with nanorod morphology of average rod diameter of ≈ 30 nm and randomly oriented, leading to large surface area as depicted in **Figure 7b(ii)**. Such novel morphology may find applications in photoelectrochemical solar cells, gas sensors and super capacitors [22].

Figure 7c(i) and **(ii)** represents the SEM micrographs of as-deposited and annealed CZO with Cu:Zn of 3%. The as-deposited film sample is identified with dense and vertically aligned nanorod morphology of varying rod sizes with average rod diameter of 120 nm and high porosity as well as high surface roughness. After post-annealing treatment at 673 K, the former nanorod morphology became fibrous, vertically aligned with well-defined and nearly uniform rod sizes (mean rod diameter of ≈ 112 nm) as depicted in **Figure 7c(ii)**. This morphology is suitable for dye-sensitized solar cell (DSSCs) application.

The SEM micrographs of CZO with Cu concentration of 5% are shown in **Figure 7d(i)** and **(ii)**. As-deposited film samples, d(i), show densely oriented nanorods. After post-annealing treatment at 673 K, dense, uniformly oriented nanorods with fine structures were obtained as in d(ii). These observations agree with that observed by Chow et al. [2] using chemical synthesis of CZO thin films and are suitable for PEC solar cell application.

3.4 Optical characterizations

The UV-Vis absorbance spectra measured in the work of Tyona et al. [10] is illustrated in **Figure 8**. The measurements were carried out in the wavelength range of 300–800 nm at room temperature, with undoped ZnO as reference. The spectra generally revealed low absorbance for all the film samples in the visible region especially the undoped ZnO and CZO samples with Cu concentrations of 1 and 5%, with sharp absorption edge at about 395 nm. An enhancement in absorption was noticed in CZO with Cu:Zn of 3%; the band edge was shifted towards lower energy at 450 nm (**Figure 8**). This is an enhancement in optical absorbance induced by Cu doping.

The optical band gap energy (E_g) was obtained from Tauc plot using Tauc's relationship between the absorption coefficient, α , and the photon energy, $h\nu$, as shown in Eq. (5) [10]:

$$\alpha = \frac{\alpha(h\nu - E_g)^n}{h\nu} \quad (5)$$

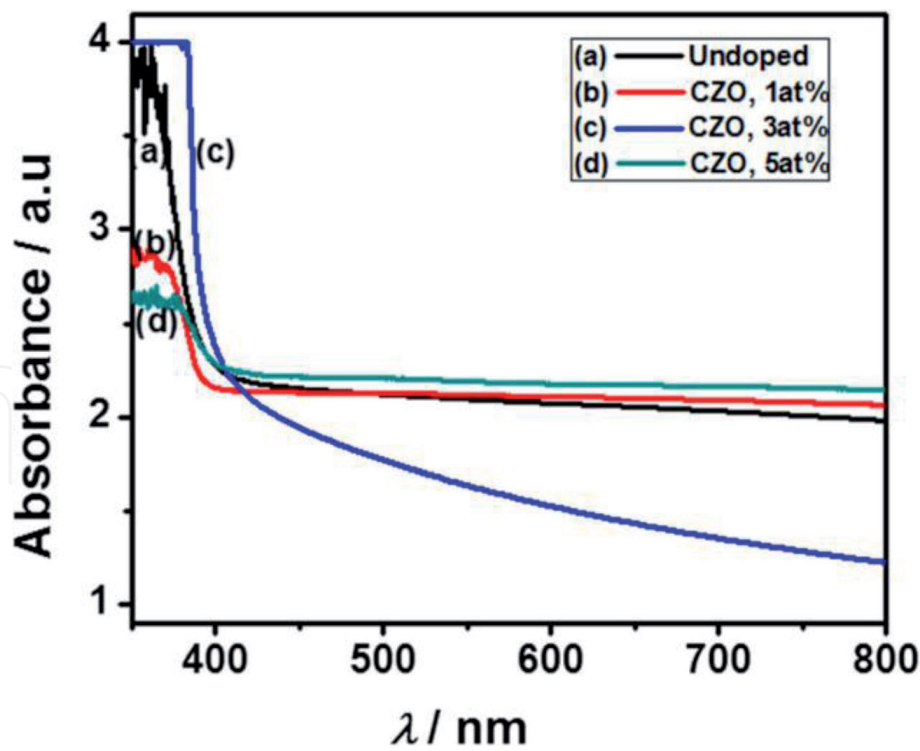


Figure 8.
Absorption spectra of CZO thin film for different Cu concentrations: (a) 0%, (b) 1%, (c) 3% and (d) 5% [10].

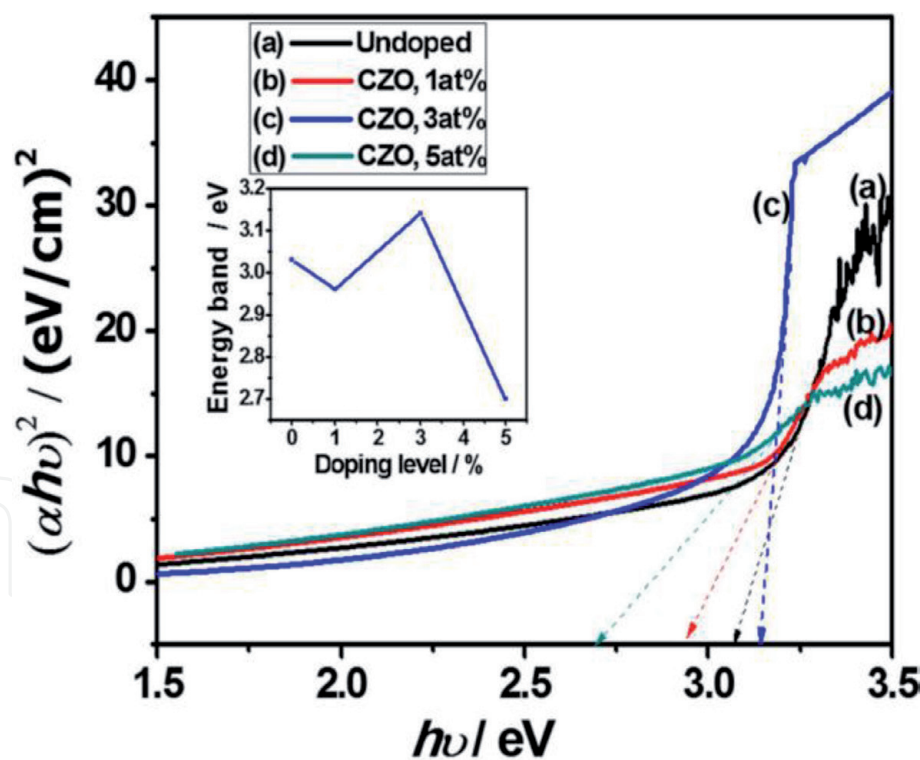


Figure 9.
Tauc plot from absorbance spectra of CZO thin film for different Cu concentrations: (a) 0%, (b) 1%, (c) 3% and (d) 5%. Inset shows the band gap trend of undoped and Cu-doped ZnO thin films [10].

where α_0 is a constant. E_g is the optical band gap and n is a constant which depends on the probability of transition (it takes values as 1/2, 3/2, 2 and 3 for direct allowed, direct forbidden, indirect allowed and indirect forbidden transition, respectively) [22]. The band gaps of the CZO thin films were estimated by extrapolating to the photon energy axis, the linear portion of Tauc's plot as depicted in Figure 9.

The estimated E_g values of CZO thin films are observed to decrease from 3.03 eV for undoped ZnO to 2.96 eV upon incorporation of Cu impurities into ZnO (1%) and later increased to 3.14 eV as the impurity concentration was raised to 3% (in set, **Figure 9**). This anomaly in band gap of CZO thin films they observed was adduced to stress incorporated in the films which resulted from some defects on Zn sites induced by Cu impurities [22]. The reduction in the band gap observed thus facilitates excitation of electrons from the valence band to conduction band, even under illumination with visible light photons. This is beneficial for achieving an improved PEC performance from an UV-active material [19]. This study confirms that the incorporation of an optimum concentration of Cu in ZnO can yield a modification in the band gap of ZnO and thus provide an efficient solar light absorbing optical system, which can be useful for the solar energy applications [26].

Optical transmittance showed variation over a wavelength range of 350–800 nm. Regardless of the Cu concentration, all films are highly transparent in the visible (400–800 nm) region. The transmittance of Cu-doped films showed moderately high values in the range of 60–90% in the visible region as shown in **Figure 10**. Upon incorporation of Cu impurities, the optical transmittance was found to decrease from 85% (undoped) to 78% (CZO, 1%); further increase in Cu concentration enhanced the transmittance value to 90%. At higher doping concentration (above 3%), the transmittance was observed to decrease with increased Cu concentration which may be adduced to decrease in crystalline quality of the Cu-doped film.

3.5 Surface wettability studies

Surface wettability involves the interaction between liquids and solids in contact. The wetting behaviour of thin film is characterized by the value of contact angle, a microscopic parameter. The contact angle is an important parameter in surface science, and its measurement provides a simple and reliable technique for

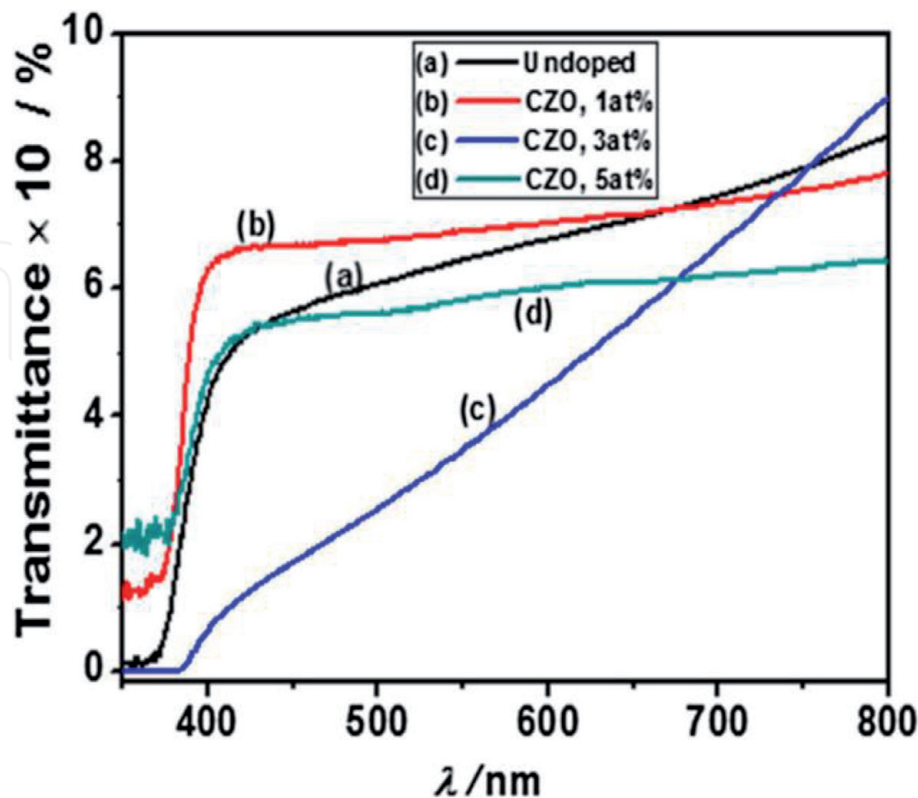


Figure 10. Transmittance spectra of CZO thin films with different Cu concentrations: (a) 0%, (b) 1%, (c) 3% and (d) 5% [10].

the interpretation of surface energies [10, 27]. The knowledge of contact angle of thin films is important for practical applications such as in DSSCs, super capacitors and gas sensing [10, 28].

Tyona et al. [10] reported water contact angles of CZO thin films as illustrated in **Figure 11a–d**. The contact angles are observed to decrease from 71.3 to 15.2° upon doping. These results showed strong dependence of the contact angles on annealing temperature as well as Cu concentration. The water contact angles decreased (as compared with undoped sample **Figure 11b**) upon incorporation of Cu impurities up to optimal percentage impurity of 3% (**Figure 11c**) and further increase as the impurity concentration was increased beyond this level (**Figure 11d**). This implies

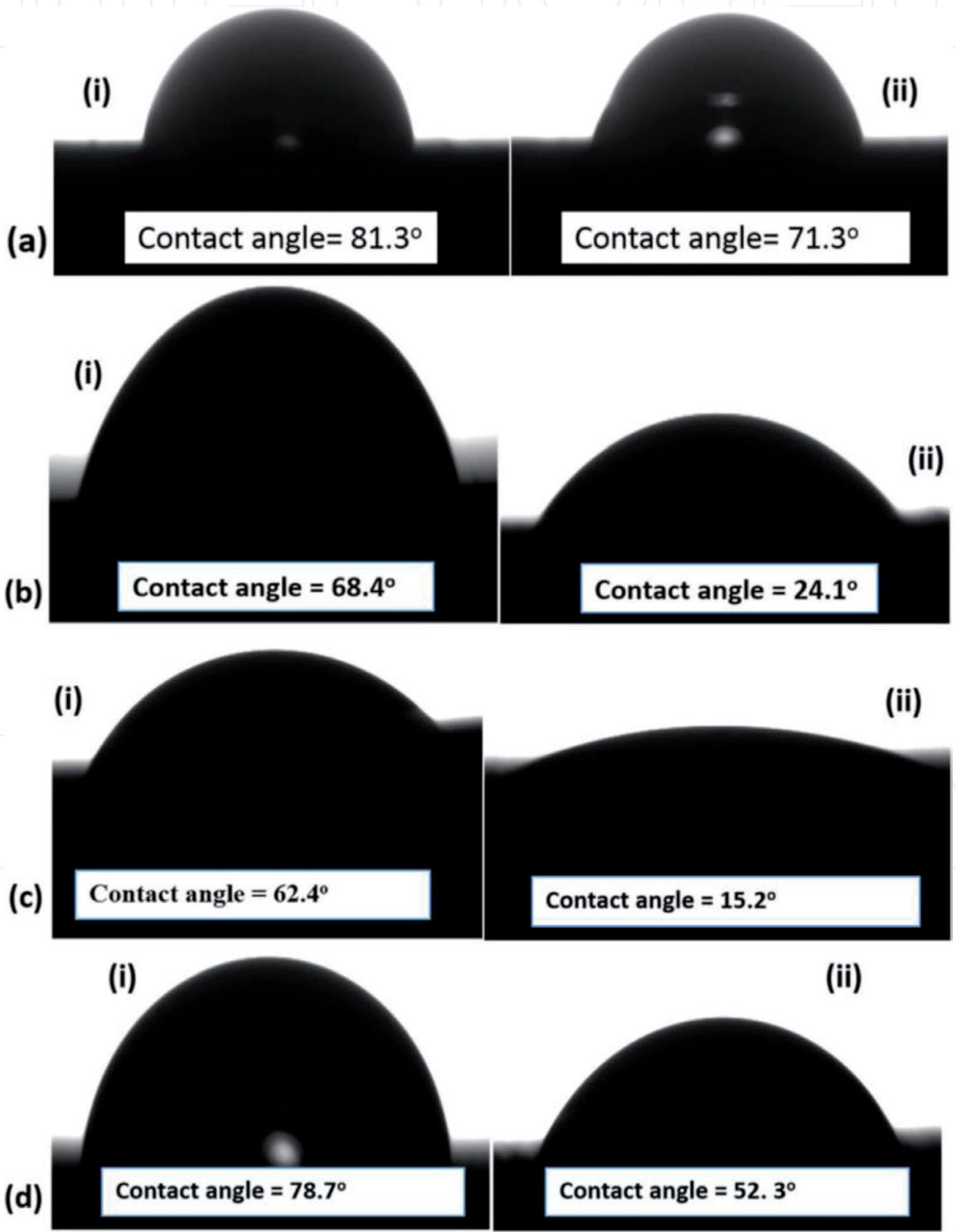


Figure 11. Water contact angles of CZO thin films showing as-deposited and annealed samples for various Cu concentrations: (a) 0%, (b) 1%, (c) 3% and (d) 5% [10]. In **Figure 11**, (i) is as deposited, (ii) is annealed.

that the porosity of the films increases upon thermal annealing at 673 K and with respect to increased concentration of Cu; thus, the water goes in to the pores and craves making contact angle hydrophilic [10, 28]. This means that the films would have large surface areas which for application such as DSSCs would mean better dye adsorption resulting to enhanced photo absorption. Also, lower values of contact angles are beneficial for electrolyte percolation through the porous film, which is very important for PEC solar cells. This result is in agreement with the earlier observations from XRD and SEM.

3.6 Photoelectrochemical (PEC) studies

Photoelectrochemical response of a solar cell is based on the junction between semiconductor and an electrolyte. The electrolyte plays an important role in PEC cell as a medium for charge transfer between the photoelectrode and counter electrode [10, 22].

The photoresponses of the CZO thin films were studied by forming typical configuration cells, n-CZO (stainless steel substrate)/0.1 M Na₂SO₄/platinum/SCE. These PEC cells are easy to form, and many processing steps of p–n junction have been simplified or eliminated. Since the junction with liquid is formed spontaneously upon contact, irregular-shaped single crystal or thin films can be used [10, 17]. The solution-based measurements allowed us to quickly test the quality of CZO film electrode as a solar cell material [10, 17].

Tyona et al. [10] reported the PEC performance of their CZO using current–voltage (I–V) characteristics of the annealed CZO thin films in the dark and under illumination with 80 mW/cm² as illustrated in **Figure 12a–c**. The anodic

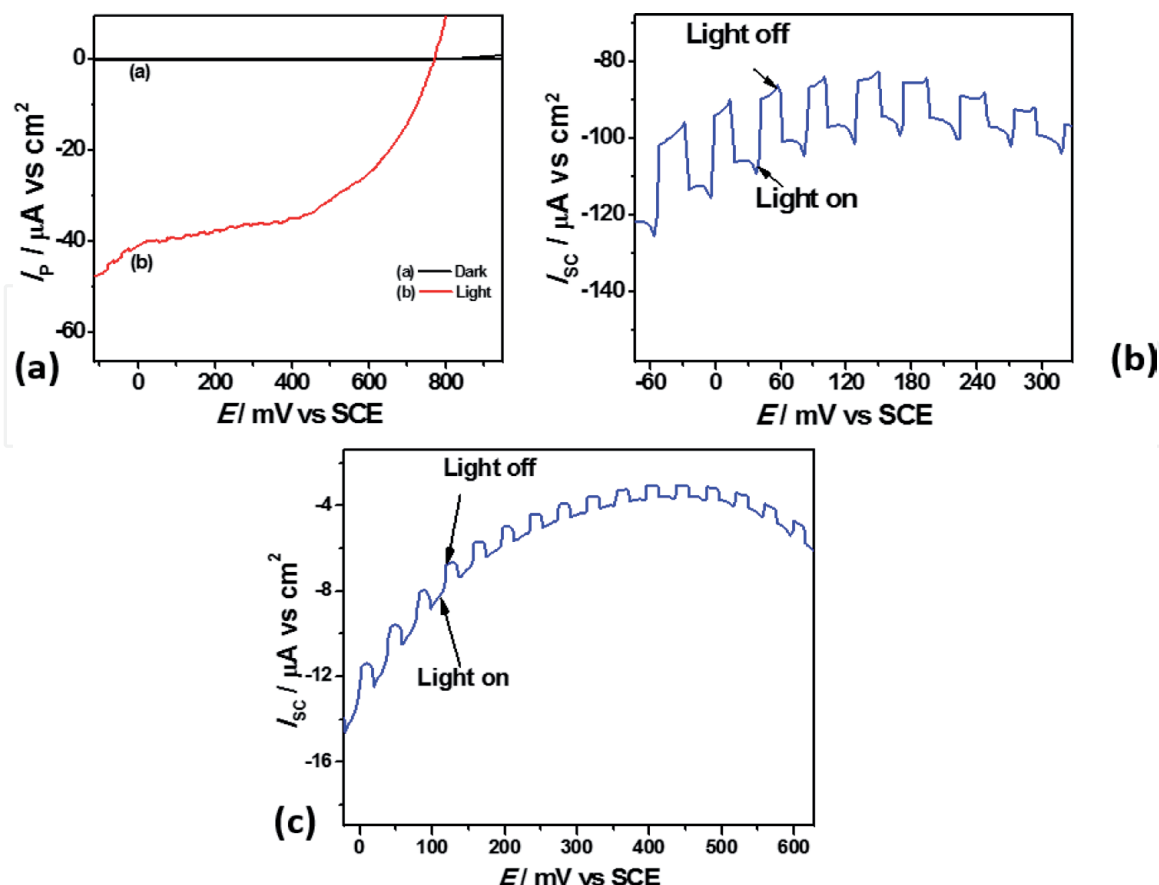


Figure 12.

Current-potential (I–V) curves of CZO thin films showing current and potential in the dark and under illumination for (a) 1%, (b) 3% and (c) 5% Cu concentrations [10].

| ZnO electrodes | Photocurrent (I_{SC}) [$\mu A/cm^2$] | Photovoltage (V_{oc}) [mV] | I_{max} ($\mu A/cm^2$) | V_{max} (mV) | Efficiency η (%) | Fill factor (FF) |
|----------------|--|--------------------------------|----------------------------|----------------|-----------------------|------------------|
| Undoped | 12.34 | 388.0 | 9.00 | 230.0 | 0.0030 | 0.43 |
| CZO (1%) | 40.00 | 774.0 | 28.00 | 631.0 | 0.0220 | 0.57 |
| CZO (3%) | 98.00 | 796.0 | 74.00 | 667.0 | 0.0620 | 0.63 |
| CZO (5%) | 16.00 | 768.0 | 13.00 | 52.0 | 0.0009 | 0.06 |

Table 2.
Values of I-V measurement from PEC cells of CZO thin films [10].

photocurrent varied remarkably with the concentration of Cu in ZnO as reported with previous characterizations of the CZO. **Figure 12b** and **c** also represents the chopped light tests carried out in order to study the photosensitivity of CZO thin films. The photosensitivity confirmed that CZO absorber is an n-type material and is useful for the solar cell [10, 17]. The measured values of the PEC parameters with respect to Cu doping are shown in **Table 2**.

The photoelectrochemical measurement confirmed good photoactivities of the annealed CZO films prepared from simple CBD method. It is however observed that the photocurrent (short circuit current, I_{SC}) conversion efficiency and fill factor of the CZO film for 5% Cu are relatively low. This may be due to more compressive strain in the films at higher doping level as earlier explained in XRD which probably leads to a less dense nanostructure as illustrated in **Figure 7d** and consequently low photoactivity. The photocurrent obtained in the present study is not useful for most practical applications requiring high values of current; however, it is well known that conversion efficiency of such film can be considerably improved by thermal, chemical and photoelectrochemical surface treatments [10, 17].

4. Conclusions

This chapter examines ZnO and its numerous nanostructures and also considered doping as a measure for engineering the properties of ZnO for pre-determined applications. The chapter has also extensively reviewed the effect of Cu doping on structural, morphological and optical properties and surface wettability of chemical bath deposited ZnO thin films at various concentrations of Cu in the range 1–5% for PEC solar cell application. The review indicated that there were slight changes in the lattice parameters of the CZO electrodes which occurred due to the successful substitution of Zn^{2+} by Cu^{2+} and also enhancement in crystalline quality of the films at 3% Cu concentration due to the reduction in crystallographic defects in the film. A review of SEM studies showed densely grown nanorods over the varied range of Cu concentration, with the CZO nanorods of 3% having the most dense microstructures with average diameter approximately 125 nm. The density and diameter of the nanostructures demonstrated dependence on the amount of Cu dopant. A review of optical properties demonstrated that the incorporation of Cu dopant into ZnO introduced a shift in absorption edge of approximately 60 nm into the visible band for the CZO nanorods with 3% Cu content which is a significant enhancement in the optical properties of the films. Also, optical energy band gaps decrease from 3.03 to 2.70 eV upon Cu doping. Surface wettability was adjudged hydrophilic for all the films, which implied high porosity, and the size of water contact angles show dependence on Cu content. Photoelectrochemical cell performance indicated an n-type photoactivity in sodium sulphate (Na_2SO_4) electrolyte which motivate to check its feasibility in solar cell applications.

Acknowledgements

I am grateful to Benue State University, Makurdi, for providing an enabling environment for this work.

Conflict of interest

I declare that there is no conflict of interest.


Author details

Tyona MD

Department of Physics, Benue State University, Makurdi, Benue State, Nigeria

*Address all correspondence to: dtyona@gmail.com; dtyona@bsum.edu.ng

IntechOpen

© 2019 The Author(s). Licensee IntechOpen. This chapter is distributed under the terms of the Creative Commons Attribution License (<http://creativecommons.org/licenses/by/3.0>), which permits unrestricted use, distribution, and reproduction in any medium, provided the original work is properly cited. 

References

- [1] Zhong LW. Zinc oxide nanostructures: Growth, properties and applications. *Journal of Physics. Condensed Matter*. 2004;**16**:R829-R858
- [2] Chow L, Lupan O, Chai G, Khallaf H, Ono L, Roldan K, et al. Synthesis and characterization of Cu-doped ZnO one-dimensional structures for miniaturized sensor applications with faster response. *Sensors and Actuators A*. 2013;**189**:399-408
- [3] Drici A, Djeteli G, Tchangbedgi G, Deruiche H, Jondo K, Napo K, et al. Structured ZnO thin films grown by chemical bath deposition for photovoltaic applications. *Physica Status Solidi (a) Banner*. 2004;**201**:1528-1535
- [4] Li Y, Gong J, Deng Y. Hierarchical structured ZnO nanorods on ZnO nanofibers and their photoresponse to UV and visible lights. *Sensors and Actuators A: Physical*. 2010;**158**:176-187
- [5] Lao CS, Liu J, Gao P, Zhang L, Davidovic D, Tummala R, et al. ZnO nanobelt/nanowire Schottky diodes formed by dielectrophoresis alignment across Au electrodes. *Nano Letters*. 2006;**6**:263-275
- [6] Tyona MD, Osuji RU, Ezema FI, Jambure SB, Lokhande CD. Enhanced photoelectrochemical solar cells based on natural dye-sensitized Al-doped zinc oxide electrodes. *Advances in Applied Science Research*. 2016;**7**:18-31
- [7] Vanaja A, Ramaraju GV, Srinivasa RK. Structural and optical investigation of Al doped ZnO nanoparticles synthesized by sol-gel process. *Indian Journal of Science and Technology*. 2016;**9**:23-28
- [8] Cebulla R, Wndt R, Ellmer K. Al-doped zinc oxide films deposited by simultaneous RF and DC excitation of a magnetron plasma: Relationships between plasma parameters and structural and electrical film properties. *Journal of Applied Physics*. 1998;**83**:1087-1095
- [9] Seshan K. *Handbook of Thin-Film Deposition Processes and Techniques: Principles, Methods, Equipment and Applications*. Second ed. New York, U.S.A: William Andrew Publishing Norwich; 2002. pp. 344-356
- [10] Tyona MD, Osuji RU, Asogwa PU, Jambure SB, Ezema FI. Structural modification and band gap tailoring of zinc oxide thin films using copper impurities. *Journal of Solid State Electrochemistry*. 2017;**21**:2629-2637
- [11] Snure M, Tiwari A. Band-gap engineering of $\text{Zn}_{1-x}\text{Ga}_x\text{O}$ nanopowders: Synthesis, structural and optical characterizations. *Journal of Applied Physics*. 2008;**104**:073707-073705
- [12] Singhal S, Kaur J, Namgyal T, Sharma R. Cu-doped ZnO nanoparticles: Synthesis, structural and electrical properties. *Physica B*. 2012;**407**:1223-1226
- [13] Dom R, Lijin RB, Kim HG, Borse PH. Enhanced solar photoelectrochemical conversion efficiency of ZnO:Cu electrodes for water-splitting application. *International Journal of Photoenergy*. 2013;**2013**:9-20
- [14] Zhou Z, Kato K, Komaki T, Yoshino M, Yukawa H, Morinaga M, et al. Electrical conductivity of Cu-doped ZnO and its change with hydrogen implantation. *Journal of Electroceramics*. 2003;**11**:73-79
- [15] Jongnavakit P, Amornpitoksuk P, Suwanboon S, Ndiege N. Preparation and photocatalytic activity of Cu-doped ZnO thin films prepared by the sol-gel method. *Applied Surface Science*. 2012;**258**:8192-8198

- [16] Tyona MD, Osuji RU, Ezema FI. A review of zinc oxide photoanode films for dye-sensitized solar cells based on zinc oxide nanostructures. *Advanced Nano Research*. 2013;**1**:43-58
- [17] Shinde NM, Dubal DP, Dhawale DS, Lokhande CD, Kim JH, Moon JH. Room temperature novel chemical synthesis of $\text{Cu}_2\text{ZnSnS}_4$ (CZTS) absorbing layer for photovoltaic application. *Materials Research Bulletin*. 2012;**47**:302-307
- [18] Machado G, Guerra DN, Leinen D, Ramos-Barrado JR, Marotti RE, Dalchiele EA. Indium doped zinc oxide thin films obtained by electrodeposition. *Thin Solid Films*. 2005;**490**:124-131
- [19] Tyona MD, Jambure SB, Lokhande CD, Banpurkar AG, Osuji RU, Ezema FI. Dye-sensitized solar cells based on Al-doped ZnO photoelectrodes sensitized with rhodamine. *Materials Letters*. 2018;**220**:281-284
- [20] Becerril M, Silva-López H, Guillén-Cervantes A, Zelaya-Ángel O. Aluminum-doped ZnO polycrystalline films prepared by co-sputtering of a ZnO-Al target. *Revista Mexicana de Física*. 2014;**60**:27-31
- [21] Muthukumaran S, Gopalakrishnan R. Structural, FTIR and photoluminescence studies of Cu doped ZnO nanopowders by coprecipitation method. *Optical Materials*. 2012;**34**:1946-1953
- [22] Babikier M, Wang D, Wang J, Li Q, Sun J, Yan Y, et al. Cu-doped ZnO nanorod arrays: The effects of copper precursor and concentration. *Nanoscale Research Letters*. 2014;**9**:199-207
- [23] Thakur S, Sharma N, Varkia A, Kumar J. Structural and optical properties of copper doped ZnO nanoparticles and thin films. *Advances in Applied Science Research*. 2014;**5**:18-24
- [24] Shannon RD. Revised effective ionic radii and systematic studies of interatomic distances in halides and chalcogenides. *Acta Crystallogr. Sect. A*. 1976;**32**:751-767
- [25] Mkawi EM, Ibrahim K, Ali MKM, Farrukh MA, Mohamed AS. The effect of dopant concentration on properties of transparent conducting Al-doped ZnO thin films for efficient $\text{Cu}_2\text{ZnSnS}_4$ thin-film solar cells prepared by electrodeposition method. *Applied Nanoscience*. 2015;**3**:56-67
- [26] Mani GK, Rayappan JBB. Influence of copper doping on structural, optical and sensing properties of spray deposited zinc oxide thin films. *Journal of Alloys and Compounds*. 2014;**582**:414-419
- [27] Sun RD, Nakajima A, Fujushima A, Watanabe T, Hashimoto K. Photoinduced surface wettability conversion of ZnO and TiO_2 thin films. *The Journal of Physical Chemistry. B*. 2001;**105**:1984-1991
- [28] Sun H, Luo M, Weng W, Cheng K, Du P, Shen G, et al. Room-temperature preparation of ZnO M nanosheets grown on Si substrates by a seed-layer assisted solution route. *Nanotechnology*. 2008;**19**:125603-125610